

1 Identifying plausible historical scenarios for coupled lake level
2 and seismicity rate changes: The case for the Dead Sea during
3 the last two millennia.

4 **Mariana Belferman¹, Amotz Agnon², Regina Katsman¹ and Zvi Ben-Avraham¹**

5 ¹ *The Dr. Moses Strauss Department of Marine Geosciences, Leon H. Charney School of Marine
6 Sciences, University of Haifa, Mt. Carmel, Haifa 3498838, Israel.*

7 ² *The Fredy & Nadine Herrmann Institute of Earth Sciences, The Hebrew University of
8 Jerusalem, Jerusalem 9190401, Israel*

9 Mariana Belferman: mkukuliev@gmail.com (corresponding author)

10 Amotz Agnon: amotz@huji.ac.il

11 Regina Katsman: rkatsman@univ.haifa.ac.il

12 Zvi Ben-Avraham: zviba@post.tau.ac.il

13 **ABSTRACT**

14 Studies of seismicity induced by water level changes in reservoirs and lakes focus typically on
15 well-documented contemporary records. Can such interactions be explored on a historical time
16 scale when the two data types suffer from severe uncertainties stemming from the different nature
17 of the data, methods, and resolution? In this study, we show a way to considerably improve the
18 correlation between interpolated records of historical Dead Sea level reconstructions and discrete
19 seismicity patterns in the area, over the period of the past two millennia. Inspired by the results of
20 our previous study, we carefully revise the historical earthquake catalog in the Dead Sea, to
21 exclude remote earthquakes, and include small local events. For addressing the uncertainties in

22 lake levels, we generate an ensemble of random interpolations of water level curves and rank them
23 by correlation with the historical records of seismic stress release. We compute a synthetic catalog
24 of earthquakes applying a Mohr-Coulomb failure criterion. The critical state of stress at
25 hypocentral depths is achieved by static poro-elastic deformations incorporating the effective
26 normal stress change (due to the best-fit water level curve) superimposed on the regional strike-
27 slip tectonic deformations. The earthquakes of this synthetic catalog show an impressive
28 agreement with historical earthquakes documented to damage Jerusalem. We refine the seismic
29 catalog by searching for small local events that toppled houses in Jerusalem; including all local
30 events improves the correlation with lake levels. We demonstrate for the first time a high
31 correlation between water level changes and the recorded recurrence intervals of historical
32 earthquakes.

33 **KEYWORDS**

34 Induced seismicity; Seismic recurrence interval; Water level changes; Effective stress; Dead Sea;
35 poro-elastic response.

36 **INTRODUCTION**

37 Earthquakes induced by water level changes in lakes and reservoirs has been a focus of
38 seismic investigations around the world (e.g. Simpson et al., 1988; Pandey and Chadha, 2003;
39 Durá-Gómez and Talwani, 2010). Triggering is attributed to a drop in the effective normal stress
40 at a fault, induced by water level change at the overlying lake's bed (Simpson et al., 1988; Durá-
41 Gómez and Talwani, 2010; Hua et al., 2013b; Gupta, 2018). This kind of triggering may be
42 particularly significant for areas with moderate and low tectonic strain accumulations (Pandey and

43 Chadha, 2003; Gupta, 2018), such as the Dead Sea fault in the Middle East (e.g., Masson et al.,
44 2015).

45 Seismic activity due to water level change was observed beneath artificial reservoirs
46 immediately after their first filling (e.g., Simpson et al., 1988; Hua et al., 2013 a). It also appeared
47 after several seasonal filling cycles (Simpson et al., 1988; Talwani, 1997), explained by diffusion
48 of pore pressure to the earthquake's hypocentral depth via the fault (Durá-Gómez and Talwani,
49 2010). In addition, reservoir-induced seismicity sometimes manifests itself at long distances away
50 from the reservoir (e.g., at 35 km, Durá-Gómez and Talwani, 2010). The correspondence of this
51 kind of contemporary seismicity to water level change is usually identified based upon real-time
52 data.

53 Alternatively, on a much longer time scale, changing seismic activity may also be associated
54 with water level changes in historical water bodies (e.g., the Dead Sea, since 2 ka, Fig. 1A, in the
55 Appendix, which occupies the tectonic depression along the Dead Sea fault). Water level hikes of
56 ~15 m, characteristic for time intervals of centuries to millennia, were analyzed in Belferman et
57 al. (2018) and shown to be able to moderate the seismicity pattern at the Dead Sea fault.

58 However, reconstruction of fluctuations in historical lake levels and the concurrent
59 seismicity are both subject to significant uncertainties. They stem from the differing nature of the
60 data gathered on these two phenomena and thus deserve special consideration. Earthquake dating
61 can be quite precise, and its accuracy is verified when different historical sources show consensus
62 (Guidoboni et al., 1994; Guidoboni and Comastri, 2005; Ambraseys, 2009). Assessment of the
63 extent of damage (hence earthquake magnitude), similarly requires such a consensus between the
64 different data sources. Sediment records can help to calibrate the analysis of the historical evidence

65 (Agnon, 2014; Kagan et al., 2011). Such records can be tested by trenching (Wechsler et al., 2014;
66 Marco and Klinger, 2014; Lefevre, 2018). However, in many cases earthquake epicenter can be
67 imprecise or not even known. Consequently, considerable uncertainty pertains to the historical
68 catalog of earthquakes related directly to the Dead Sea.

69 By contrast, historical water level records are quite precise elevation wise, as they are
70 obtained from different points around the lake (Bookman et al., 2004; Migowski et al., 2006).
71 However, water level dating could have an error of about ± 45 yr, as estimated from the radiocarbon
72 dating of shoreline deposits in fan delta outcrops (Bookman et al., 2004). This may underestimate
73 the actual dating uncertainty due to reworking of organic matter, sometimes re-deposited a century
74 or more after equilibration with the atmosphere (Migowski et al., 2004). In addition, the entire past
75 bi-millennial Dead Sea level record is constrained by less than twenty “anchor points” (the data
76 obtained by the dating collected from surveyed paleo-shorelines, Bookman et al., 2004). Therefore,
77 its continuous reconstruction, as suggested in the literature (Migowski et al., 2006; Stern, 2010),
78 usually takes different forms within the acceptable limits dictated by the evidence,
79 geomorphological (Bookman et al., 2004) and limnological (Migowski et al., 2006). A challenging
80 uncertainty for our study arises from the interpolations required for periods when the available
81 data do not constrain the water levels.

82 In this article, we take advantage of the correlation between the historical water level (WL)
83 reconstructions at the Dead Sea and seismicity patterns in the area over the past two millennia. We
84 demonstrate for the first time that plausible scenarios for the lake level history can fit very well
85 the record of the historical earthquake recurrence intervals (RIs). Based on the correlation between
86 these phenomena, we offer an alternative explanation regarding the triggering of earthquakes in
87 the area of the Dead Sea.

88 **METHODS**

89 To investigate the relationship between an accurate but discrete chronology of earthquakes
90 and the continuous water WL change, we first explore the space of possible WL histories by a
91 statistical approach. We generate an ensemble of WL curves (based on the anchor points, Bookman
92 et al., 2004), while remaining within the limits dictated by climatic and morphological constraints
93 (Bookman et al., 2004; Migowski et al., 2006; Stern, 2010), by using a random number generator.

94 In our analysis we associate all the historical earthquakes presented (Table 1A,2A in
95 Appendix) with rupture of the strike-slip faults, which agree with our modeling approach. Hence,
96 the major strike-slip faults constituting the plate boundary (Lower Jordan fault, Dead Sea Lake
97 fault and Northern Arava) could be affected by Dead Sea WL changes. Therefore, our study covers
98 the area within this distance

99 **A best fit random method of WL curve prediction**

100 The compilation of WL curves of the Dead Sea for the last two millennia from three recent
101 publications (Bookman et al., 2004; Migowski et al., 2006 and Stern 2010) is presented in Figure
102 1A by dashed curves. Generally, the differences between all dashed curves at anchor points is
103 included within an error limit of ± 45 yr as indicated by error bars, with an exception of the anchor
104 point dated to 1400 CE (Bookman et al., 2004) for which Migowski et al. (2006) and Stern (2010)
105 suggested a higher WL. Nevertheless, each hypothetical WL curve is forced to pass through all
106 anchor points provided by Bookman et al. (2004) except for one, at around 500 CE. The WL drop
107 around this time, according to Migowski et al. (2006) and Stern (2010), occurred later than was
108 originally suggested by Bookman et al. (2004) (Figure 1A). Because this shift is within the
109 permissible error limits (± 45 yr), this anchor point is shifted to the left (+40 yr). In addition, the

110 WL determined on the curve edges of the studied bi-millennial time interval was defined by
111 additional two anchor points, through which the estimated WL curve passed according to all three
112 references. In total, we have 13 anchor points. Between each pair of points, the trends in the WLs
113 are constrained by the sedimentary facies (Migowski et al., 2006) that specify the edge points of
114 the interval as the extrema for the acceptable WL variation.

115 However, within the largest interval between the anchor points (600 - 1100 CE), the field
116 studies (Migowski et al., 2006; Stern, 2010; Bookman et al., 2004) constrained the WL to be lower
117 than the extrema at the edges of that interval. For this period, the WL was randomly interpolated
118 between the higher (e.g., Migowski et al., 2006) and lower (e.g., Stern, 2010) bounds. To maintain
119 a monotony of the WL variation (required by the facies analysis of Migowski et al.), a moving
120 average filtered the random noise between every pair of the anchor points. Accounting for the
121 above-mentioned limits, and setting a ten-year step, the model has generated 10 million WL curves
122 for the last bimillennial interval, using a uniformly distributed random number generator.

123 We test for linear correlation between the RIs of the widely recorded moderate-to-large
124 ($M > 5.5$) historical earthquakes available from the literature (Table 1 and the text description in
125 Appendix), and the WL interpolations (as in Figure 9 in Belferman et al., 2018); and evaluate the
126 values of the Pearson product-moment correlation coefficient, R (Figure 1B). We use this statistic
127 for evaluating the suitability of each randomly interpolated WL curve for our analysis, for
128 identification and elimination of any outliers, and for studying the behavior of the entire ensemble
129 of the curves generated.

130 **The earthquake simulation algorithm**

131 The most suitable WL curve suggested by this correlation (discussed in the results section
 132 below), was used to generate a “synthetic” earthquake catalog based on the algorithm described in
 133 this section. Effective (normal) poroelastic stress change due to the WL change is superimposed
 134 on the tectonic stress accumulated consistently with the slip rate since the preceding seismic event,
 135 and synthetic earthquakes are simulated using a Coulomb failure envelope and a Mohr circle (e.g.
 136 Jaeger et al., 2009). A vertical strike-slip fault below the lake/reservoir bed is assumed (simulating
 137 a Dead Sea fault), embedded in the 2D (plain strain) geometry of the upper crust (Belferman et al.,
 138 2018). Tectonic horizontal strike-slip displacements across the fault are approximated by a simple
 139 shear approach with no normal strain component.

140 In the poroelastic part of the model, horizontal stress change normal to the strike slip fault
 141 produced by the WL change, is calculated under a uniaxial (vertical) strain condition (Eq.10b in
 142 Belferman et al., 2018). This is applicable to a post-diffusion stage: i.e., when pore pressure at
 143 hypocentral depth equilibrates with the lake’s bed. An array of the effective horizontal normal
 144 stress changes, $\Delta\sigma'_i$, at the fault, induced by the water load change at the lake’s bed, p_{s_i} ,
 145 corresponds to the array of the WL change, $\Delta h_i (i = 1, 2, \dots, 2000)$ over the interpolated WL curve,
 146 Figure 1D:

147 1.
$$\Delta\sigma'_i = \frac{1-2\nu}{1-\nu} (\beta - 1) p_{s_i}$$

148 (Eq. 10b in Belferman et al., 2018). Here β is Biot's coefficient and ν is the Poisson’s ratio, $p_{s_i} =$
 149 $\rho g \Delta h_i$, where ρ is the density of water and g is the acceleration of gravity.

150 A radius and a center location of the Mohr circle change as a function of the tectonic
 151 deformations and WL changes, correspondingly, eventually reaching a failure envelope that
 152 simulates an earthquake. The model uses a Byerlee's law envelope (Byerlee, 1978) to define a

153 residual strength of a seismogenic zone at the fault immediately after the earthquake (Belferman
 154 et al., 2018 for more detail). Since the effective stress upon the onset of an earthquake is specified
 155 by a high failure envelope and the effective stress following the slip is given by Byerlee's law
 156 (e.g., Belferman et al., 2018), the model is time-predictable. The stress drop, at least in the
 157 nucleation zone of a single-fault model, is expected to be proportional to the RI.

158 A starting point of the simulations is the date of the first historical earthquake (33CE,
 159 Table 1 in the Appendix) from the bi-millennial time interval studied. The simulation
 160 incrementally proceeds with time over the WL curve generated (as above) under the accumulating
 161 tectonic stress. After each stress release, the time to the next earthquake, Δt , is calculated from the
 162 solution of the Mohr-Coulomb failure criterion for a strike-slip tectonic regime and a WL change,
 163 Δh_i , characteristic of the Dead Sea fault (Belferman, et al., 2018):

$$164 \quad 2. \quad (\tau_i - \tau_0)^2 + (\sigma_i - (\sigma_0 + \Delta\sigma'_i))^2 = (R_0 + \Delta\tau_{xy_i})^2$$

$$165 \quad \tau_i = C + \tan(\varphi)\sigma_i$$

166 assuming that $\Delta\tau_{xy_i} = \frac{C\cos(\varphi)}{t_{RI}}\Delta t$ is the tectonic shear stress accumulated consistently with slip-
 167 rate at the strike-slip fault during the period Δt (time passed since the last earthquake), C is
 168 cohesion, φ is an angle of internal friction, σ_0 and τ_0 are the coordinates of the Mohr circle center
 169 immediately after the earthquake and R_0 its radius, t_{RI} is the reference RI corresponding to the
 170 minimal WL.

171 For each time step, the algorithm determines whether there is a single solution, or two, or
 172 nil. A case of no solutions means that the Mohr circle is yet to reach the failure envelope, as the
 173 accumulating tectonic stress and the WL increase are still insufficient. The system of Eq. 2 may

174 have a single solution when the failure criterion is met at the end of some timestep, or two solutions
 175 when it is met before the end of the timestep. A case of two solutions is rounded down to a case
 176 of a single solution if a time step (one year) is small compared to the earthquake RI (several
 177 hundreds of years).

178 This solution of Eq.2 yields a RI as a function of the effective normal horizontal stress
 179 change, $\Delta\sigma'_i$ (Belferman et al., 2018):

$$180 \quad 3. \quad RI = \Delta t = (C + \tan(\varphi)\Delta\sigma'_i) \frac{t_{RI}}{C}$$

181 where t_{RI} is the reference RI corresponding to the minimal WL, C is cohesion, φ is an angle of
 182 internal friction. From this formula, an array of earthquake dates is obtained.

183 Substitution of Eq.1 into Eq.3, yields a linear dependence of a simulated RI on a WL change, Δh_i ,
 184 evolving with time.

$$185 \quad 4. \quad RI = t_{RI} + \frac{\tan(\varphi)}{C} \frac{1-2\nu}{1-\nu} (\beta - 1) \rho g t_{RI} \Delta h_i$$

186 A tectonic slip-rate is set at 5 mm/yr (e.g. Hamiel et al., 2018; Hamiel and Piatibratova, 2019;
 187 Masson et al., 2015). Coefficients for the simulations were previously determined in Belferman et
 188 al. (2018). Note that the cohesion, C , is not a-priori known, hence it is fixed by the empirical
 189 correlation between WL and RI for a given lake level history considered. Its value, $C = 0.08Mpa$,
 190 and a reference RI, $t_{RI} = 300yr$, were adjusted numerically for a WL curve, providing the average
 191 RI of 144 yr over the modeled period of two millennia justified by historical, archaeological, and
 192 geological data (Agnon, 2014).

193 **RESULTS**

194 Ten most suitable WL curves are identified out of the 10M set of WL randomly generated
195 curves (“ensemble”) by the Pearson product-moment correlation test. The values of the correlation
196 coefficients, R , for the entire ensemble are distributed normally around $R=0.63$ (Figure 1B) with
197 a standard deviation of $\sigma =0.076$. The ten most suitable WL curves ordered by their correlation
198 coefficients, R , are presented in Figure 2.

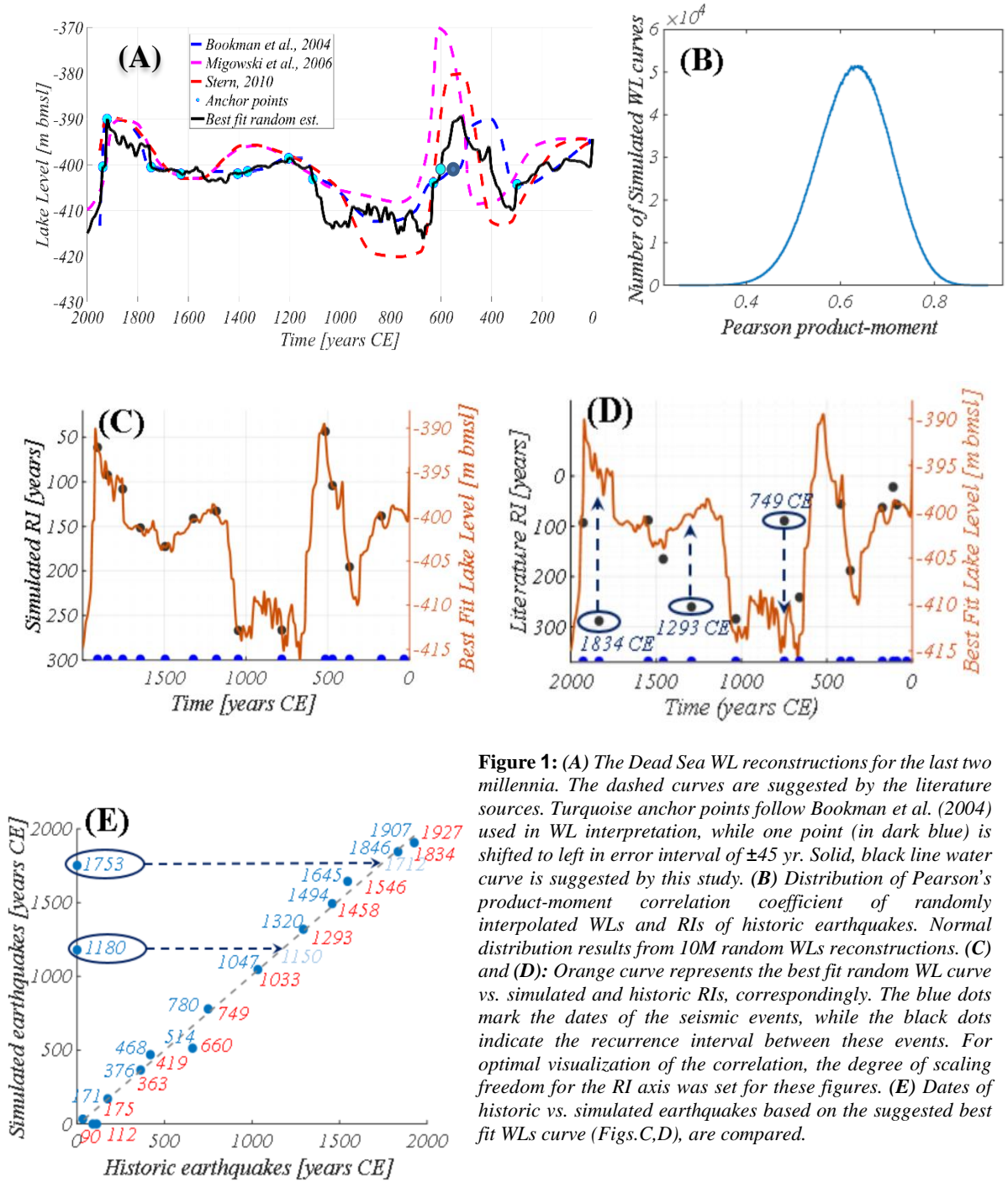
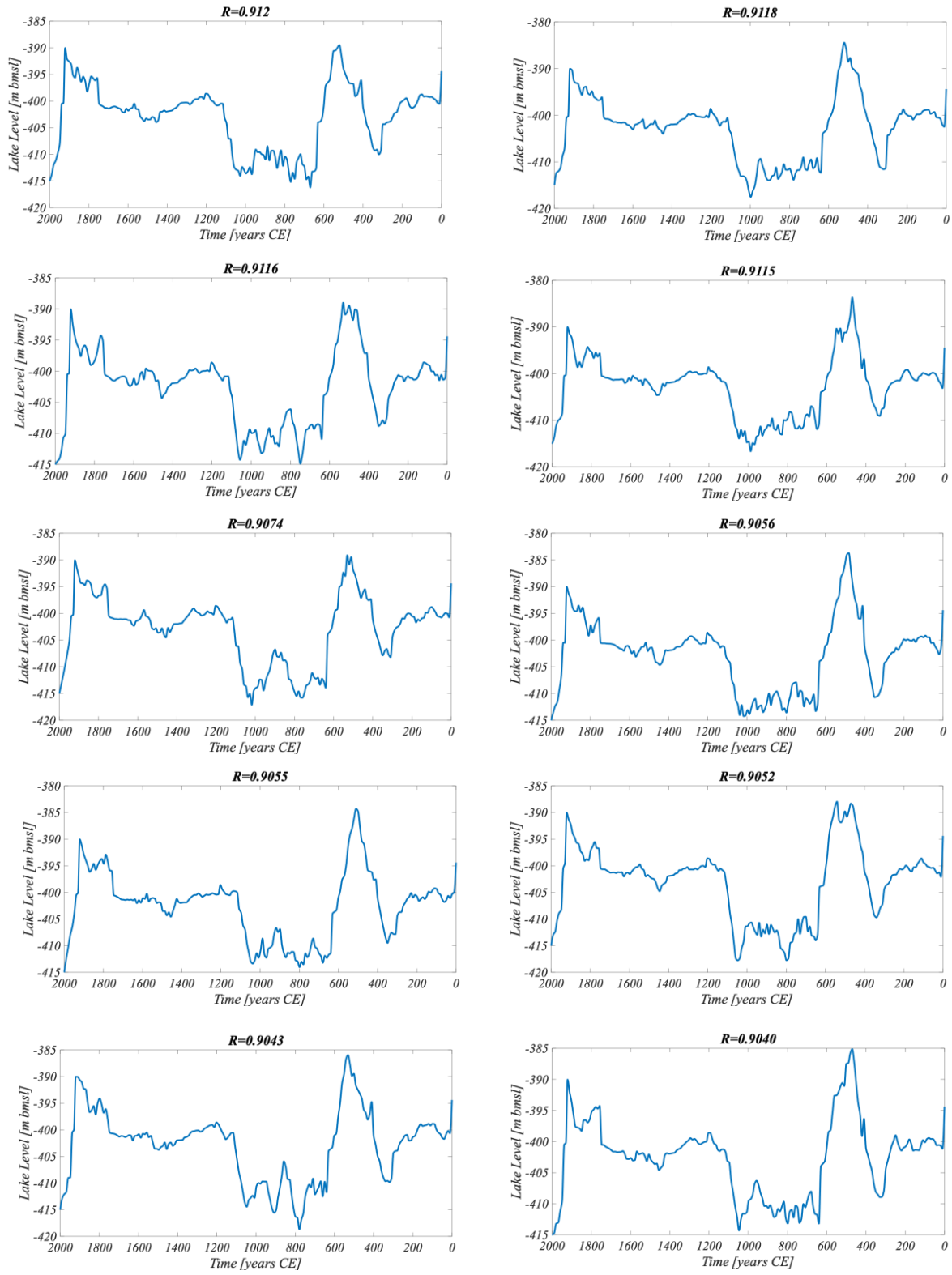


Figure 1: (A) The Dead Sea WL reconstructions for the last two millennia. The dashed curves are suggested by the literature sources. Turquoise anchor points follow Bookman et al. (2004) used in WL interpretation, while one point (in dark blue) is shifted to left in error interval of ± 45 yr. Solid, black line water curve is suggested by this study. (B) Distribution of Pearson's product-moment correlation coefficient of randomly interpolated WLs and RIs of historic earthquakes. Normal distribution results from 10M random WLs reconstructions. (C) and (D): Orange curve represents the best fit random WL curve vs. simulated and historic RIs, correspondingly. The blue dots mark the dates of the seismic events, while the black dots indicate the recurrence interval between these events. For optimal visualization of the correlation, the degree of scaling freedom for the RI axis was set for these figures. (E) Dates of historic vs. simulated earthquakes based on the suggested best fit WLs curve (Figs.C,D), are compared.



200

201

Figure 2: Ten most suitable WLs identified out of the 10M randomly generated by the Pearson product-moment correlation test.

202 Three outliers from the thirteen RIs of the widely recorded historic earthquakes (749 CE,
203 1293 CE and 1834 CE in Figure 1) were identified and reevaluated (explanation in Appendix). A
204 curve with the highest Pearson coefficient of $R=0.912$ was chosen from the correlation between
205 the RIs of the revised historic catalog and the randomly generated WLs (Figure 2). This correlation
206 can be specified by a linear prediction function:

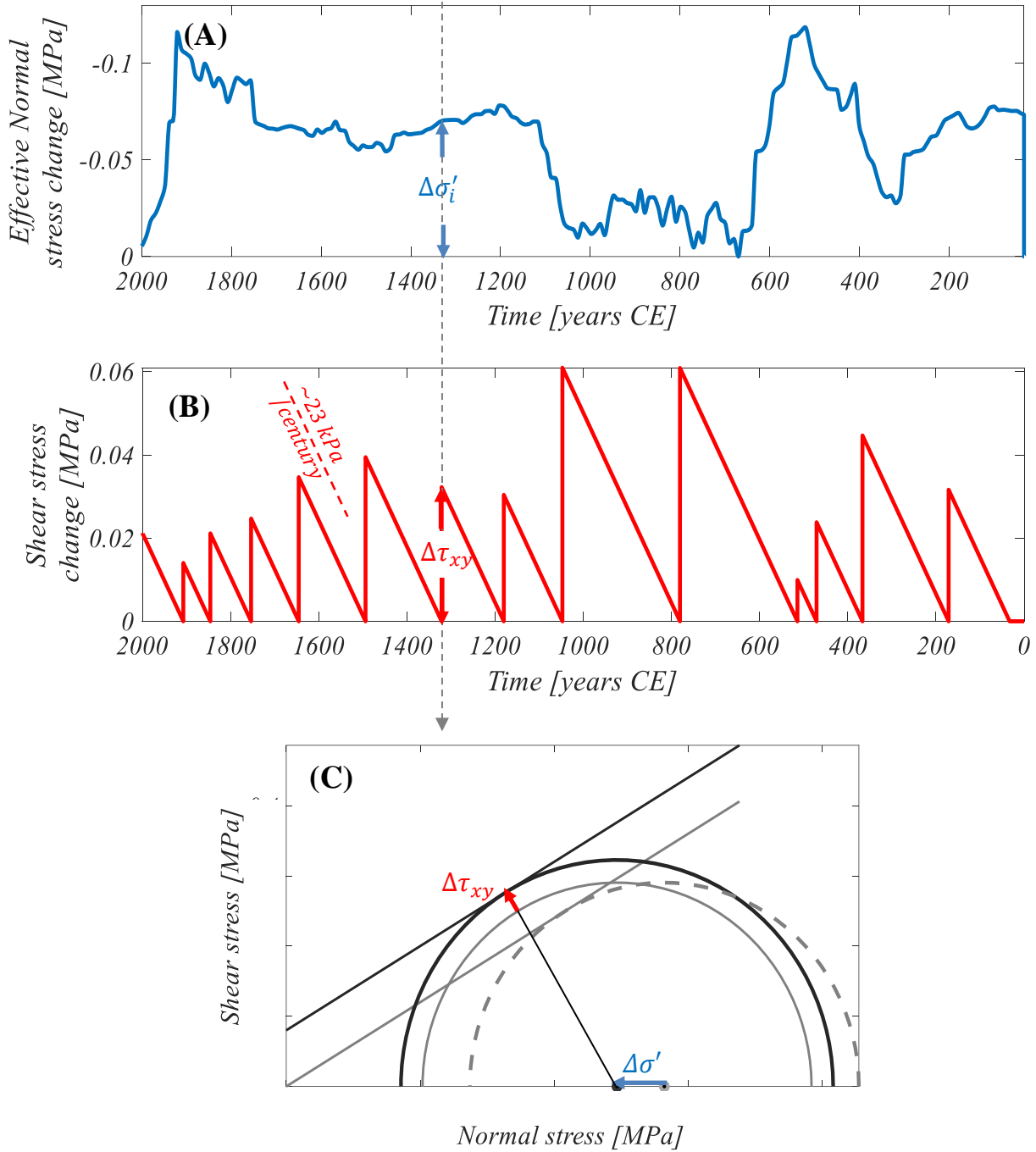
207 5. $RI = -5442 - 14WL$

208 where RI is given in years and WL in meters. In addition, a synthetic earthquake history including
209 14 seismic events was simulated from the best fit randomly interpolated WL curve with $R=1$
210 specified above. The synthetic RIs can be approximated based on the WLs using the linear
211 relationship Eq.4):

212 6. $RI = -3840 - 10WL$

213 The dates of the simulated synthetic earthquakes are presented, versus the dates of the historical
214 earthquakes from the literature (Table A1, Appendix) in Figure 1E.

215 The synthetic earthquake stress history is presented in Figure 3. The effective horizontal
216 normal stress change, $\Delta\sigma'_i$, (Figure 3A) linearly depends on the WL (Eq.1.), and as expected,
217 follows its variability. The tectonic shear stress change, $\Delta\tau_{xy}$, drops to zero after the accumulated
218 shear stress is released by the strike-slip earthquake (Figure 3B). Less shear stress is required to
219 induce the earthquake when the change in WL is larger (Figures 3A,3B), modeled with Mohr-
220 Coulomb failure criteria (Figure 3C) (explained also in Belferman et. al., 2018).



221 **Figure 3:** (A) The effective normal stress change, $\Delta\sigma'$, induced by WL change, Eq.1. (B) Tectonic shear stress change, $\Delta\tau_{xy}$,
 222 accumulated consistently with slip-rate on the strike-slip fault during the time passed since the last earthquake. The shear stress
 223 accumulation rate, used in this study is about 23 kPa/century (formulation below Eq. 2, following Belferman et al., 2018) (C)
 224 Evolution of the stress change on the fault due to combined tectonic and water loading. The state of the effective stress at the fault
 225 immediately after an earthquake is restricted by the Byerlee's law envelope with zero cohesion, $C=0$, and a friction angle, $\varphi =$
 226 0.54° . The center of the Mohr circle is located at $(\sigma_0, \tau_0=0)$ see Belferman et al., 2018 for more detail). The failure envelope is
 227 defined by $C \geq 0$ and $\varphi = 0.54^\circ$. The left shift in the center of the circle by $\Delta\sigma'$ represents pore pressure (due to WL) change at this
 228 moment (Fig.3A); the increase in radius represents tectonic shear stress, $\Delta\tau_{xy}$, accumulated during the inter-seismic period
 229 (Fig.3B). Failure occurs when the circle tangents the failure envelope (presented here for the representative 1320 CE earthquake).

230 **DISCUSSION**

231 Uncertainties in the WL reconstructions associated with dating and resolution lead to
232 considerable variance in possible interpolations (Figure 1B). A Pearson correlation coefficient test
233 shows that most of the randomly interpolated WL curves give linear correlation with earthquake
234 RIs (indicated by a mean Pearson coefficient of $R=0.63$), excluding the three outliers (Figure 1D)
235 to be discussed below. Figure 2 shows a similar pattern of the WL change for the ten most
236 correlated curves. In all cases, a significant rise in the WL of about 400 CE and 1100 CE is visible
237 and a decrease in the WL around 200 and 600 CE. Also, the maximum level around 500 and 1900
238 CE appears in all ten cases.

239 For simulating synthetic earthquakes triggered by the WL change, we use the WL curve that
240 generates the highest correlation with the revised historical catalog ($R = 0.912$) (Figure 2). The
241 dates of these simulated synthetic earthquakes are comparable with historical earthquakes (Figure
242 1E) excluding two events, whose date labels are offset to the y-axis for clarity of presentation
243 (1753 CE, 1180 CE). The dates of these synthetic earthquakes might be connected to three outliers
244 from the historical catalog (1834 CE, 1293 CE and 749 CE depicted in Figure 1D) as explained
245 below.

246 The 1180 CE synthetic earthquake (Figure 1E) is comparable to an earthquake in the
247 literature dated by Ben-Menachem (1979) and Amiran et al. (1994) to the mid-12th century (~1150
248 CE). Ambraseys (2009) doubted the precise dating but accepted this mid-12th century estimate.
249 The damaged area of this earthquake spanned Jericho and Jerusalem, and the event could be
250 considered significant because it led to the total destruction of two monasteries, one of which is
251 10 km south of Jerusalem's curtain wall. By admitting the ~1150 CE earthquake to the amended

252 catalog, we reduce the RI of the subsequent earthquake at 1293 CE (Figure 1D) from 260 to 143
253 yrs, thereby bringing this outlier very close to the linear correlation.

254 Our model also generates an earthquake in the 18th century, dated 1753 CE, for which there
255 were no matches in our initial historical catalog (Belferman et al., 2018). However, in Amiran's et
256 al. (1994) catalog an earthquake in 1712 CE is indicated: 'The quake shook the solid houses and
257 ruined three Turkish houses. Felt in Ramle, but not in Jaffa'. Additionally, this earthquake is
258 evidenced by seismites dated to 1700 – 1712 CE from an Ein Gedi site (Migowski et al., 2004).

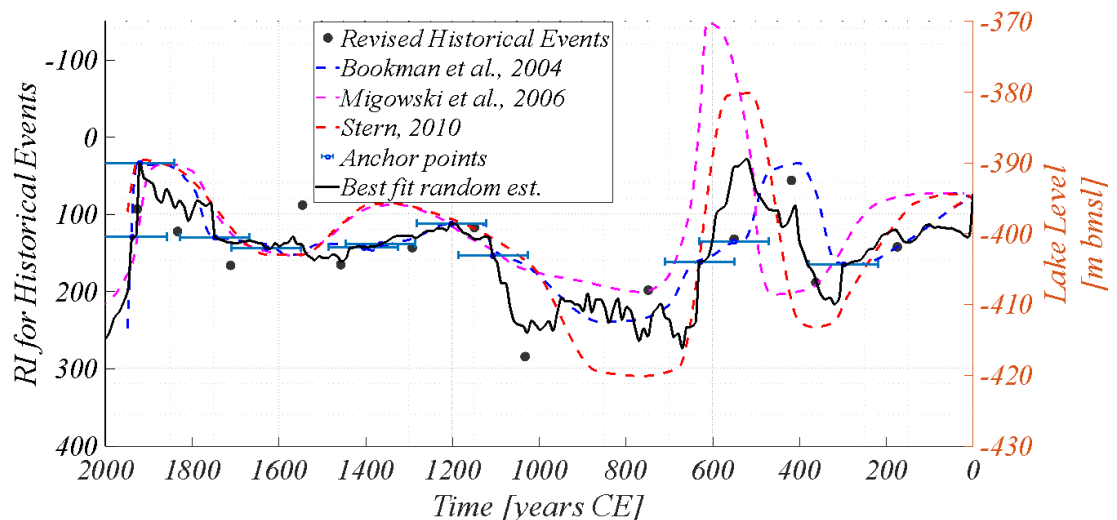
259 Regarding the modeled 1907 CE event, we note the well-documented (although often
260 overlooked) 29 March 1903 CE earthquake (Amiran et al., 1994). This was a moderate but
261 prolonged earthquake: local intensity reached VII in a number of localities distributed outside the
262 rift valley over an area of 140x70 square km (including Jerusalem), whereas the maximum
263 intensity reported in the rift was VII as well (Jericho). We prefer to correlate the modeled 1907
264 event with the stronger 1927 Jericho earthquake that clearly released stress in the Dead Sea (e.g.
265 Shapira, et al., 1993; Avni et al., 2002; Agnon, 2014). This leaves the 1903 CE unmatched to our
266 model. Perhaps the earthquake ruptured the northern part of the central Jordan Valley, north of the
267 Dead Sea and south of Lake Kinneret (Sea of Galilee).

268 Regarding the last outlier from the historical earthquakes dated to 749 CE (or its neighbors
269 747 and 757, Table A1 in the Appendix) (Figure 1D) and corresponding to the simulated 780 CE
270 earthquake (Figure 1E): the simulation generated the preceding earthquake 514 CE associated with
271 the 659/660 CE event from the literature (Table A1 in the Appendix) with a deviation of 146 years.
272 The rupture zone of the 659/660 CE event is uncertain, and this earthquake is not necessarily
273 related to stress-release at the Dead Sea basin. Alternatively, following Russell (1985), as a result

274 of the 551 CE earthquake, a fortress east of the southern Dead Sea and Petra were destroyed.
 275 Newer data contradicts the assertion regarding Petra; a failure in the Dead Sea region is still
 276 plausible. Replacing the 660 CE earthquake with 551 CE in the catalog changes the RI preceding
 277 the 749 CE historical earthquake from 89 to 198, which brings this outlier into a satisfactory linear
 278 correlation (Figure 1D).

279 Additionally, it should be emphasized that in the simulation presented in this article, the
 280 starting point is quite arbitrarily, the earthquake of 33 CE. This event together with the subsequent
 281 earthquakes 90 CE and 112 CE (not predicted by our model) span a single century where the
 282 catalog is nebulous. Each of these events could thus represent the starting point of the simulations
 283 or could be omitted at this early and poorly documented interval.

284 Summarizing the above amendments, we add to our catalog of historical events the 551 CE,
 285 ~1150 CE and 1712 CE earthquakes, and remove 559/660 CE and 90 CE, 112 CE earthquakes
 286 (Figure 1E). Altogether, we get 14 triggered historical earthquakes. The correlation between the
 287 WL and RI is noticeable for the various variants of the WL curve reconstruction (Figure 4).



288

289 **Figure 4.** *The Dead Sea WL reconstruction for the last two millennia. The dashed curves are suggested by the literature. Blue*
290 *anchor points with an error interval of ± 45 yr. follow Bookman et al. (2004). The solid black line is the WL curve suggested by this*
291 *study. The black points represent the RI for revised historical events, suggested in this study as being relevant to the Dead Sea*
292 *area.*

293 The correlation of RI with the best fit random estimated curve can be specified by a linear
294 prediction function:

295 7.
$$RI = -2483 - 6.5WL$$

296 This linear relationship between WL and RI underscores the previously proposed
297 correlations between these phenomena (in Figure 9 in Belferman et al., 2018).

298 Since the last earthquake (1927 CE), the WL in the Dead Sea has continuously decreased at
299 an average annual rate of ~ 1 m/yr. Today the WL is about -440 (m bmsl), thus our prediction
300 function (Eq. 7) suggests a RI of 377 yr, for such a WL. Namely, should the WL in the Dead Sea
301 remain constant (-440 m bmsl), as intended in some mitigation plans, we would expect the next
302 earthquake at about ~ 2300 CE.

303 This paper stresses that reconstruction of WL curves is not unique and may take various
304 forms under the constraints available (e.g., Figure 1A). However, the correlation with an
305 independent record of RIs of seismic events, assuming that earthquakes are affected by WL hikes,
306 allows deciphering plausible scenarios for WL evolution. Moreover, for cases with the best but
307 not perfect correlation, the deviation might be consistent with a release of elastic energy by smaller
308 earthquakes, which are not accounted for by the deterministic part of our model. We note that
309 smaller earthquakes might rupture dip-slip fault planes, again not accounted for by our simple
310 model.

311 Additionally, as large earthquakes are accompanied by aftershocks, some of the elastic
312 energy is released by them. It was shown earlier that in areas of reservoir-induced seismicity,
313 earthquakes are not only accompanied by aftershocks but also preceded by foreshocks (Gupta,
314 2002). The decay curve of this kind of seismicity satisfies the criteria for the second class of
315 earthquake sequences by Mogi (1963). The lack of instrumental records of historical earthquakes
316 in our study area does not allow comparison with this class. The 1995 Gulf of Aqaba earthquake
317 (7.2 Mw), the last large instrumentally recorded earthquake, was accompanied by a long period
318 (significant enough for stress release consideration) of the aftershocks. The earthquake occurred
319 along the southern part of the plate boundary, which is far enough from the Dead Sea, and most
320 likely is not influenced by the WL change. Following this earthquake felt aftershocks continued
321 for about two years. At least 50 percent of the total moment associated with these aftershocks was
322 released during the first day after the main shock and over 95 percent in the first 3 months (Baer,
323 2008). In total, the post-seismic moment released during the period of 6 months to 2 yr after the
324 Nuweiba earthquake is about 15 percent of the co-seismic moment release (Baer, 2008). This
325 earthquake showed that the response of the crust to earthquakes by aftershocks is negligible, as
326 noted for many large earthquakes (e.g., Scholz, 1972).

327 For the case of artificial reservoirs, it was shown that for reservoir-induced seismicity
328 sequences, aftershocks continue for a longer time than for tectonic earthquake sequences (Gupta,
329 2002). However, given the time scale of RI, the period of aftershocks is insufficient to consider
330 earthquakes from the sequence in our model as separate events. Regarding the time scale presented
331 in our study, when the minimal inter-seismic period is about 50 years, the stress released during a
332 post-seismic period can be considered a part of the main shock.

333 The mechanical model used in this article is rather simplistic, where earthquakes release the
334 strike-slip component of the tectonic loading (Figure 3B). The basins around the Dead Sea fault
335 system also testify for an extensional component that could be manifested in co-seismic motion
336 along normal faults. To justify our focus on a single type of fault (strike-slip), we list the following
337 arguments:

338 • The far-field maximal and minimal principal stresses in the Dead Sea region are horizontal
339 (Hofstetter et al., 2007; Palano et al. 2013). This is compatible with the dominance of
340 strike-slip faulting (Anderson, 1951). The tectonic motion at the DSF is characterized
341 predominantly by a left-lateral strike-slip regime with a velocity of ~5 mm/yr along various
342 segments (Garfunkel, 2014; Masson et al., 2015; Sadeh et al., 2012). Large earthquakes that
343 initiate clusters are likely to rupture along the straight ~100 km strike-slip segments
344 (Lyakhovsky et al., 2001). The strike of these segments parallels the relative plate velocity
345 vector and thus can be approximated by simple shear. Additionally, in the Dead Sea basin,
346 GPS surveys indicate the dominance of strike-slip loading. Hamiel et al. (2018) show that,
347 on a plate scale, horizontal shear loading dominates the velocity north of the lake. Hamiel
348 and Piatibratova (2019) detected a sub-mm/yr component of extension across the southern
349 normal fault bounding the Dead Sea pull-apart (Amatzyahu Fault); yet the strike-slip
350 component across this very fault is much larger.

351 • Normal, as well as strike-slip faults, similarly react to WL change that contributes to the
352 vertical stress component and pore pressure change. The seismicity induced by surface WL
353 fluctuations and affected by the faulting regime is critically determined by the relative
354 orientations of the three principal stresses in the Earth's crust (Anderson, 1951). In regions
355 where the vertical compressive stress is not minimal (normal and strike-slip faulting),

356 seismic activity is more sensitive to the effective stress change due to WL change, than in
357 regions where it is minimal (thrust faulting) (Simpson, 1976; Snow, 1982; Roeloffs,
358 1988). This is applicable to reservoirs approximated as “infinite” in the horizontal plane
359 (e.g., Wang, 2000), with respect to the fault zone horizontal cross-section. Since we are
360 using a one-dimensional model, such approximation is valid for our study area where the
361 Dead Sea is large enough in a horizontal plane (100 km x 10 km) compared to the thickness
362 of the underlying strike-slip fault (cross-section) located in the central part of the valley.

363 Our results demonstrate that a fairly simple forward model (based on 1D analytical
364 solution, Belferman et al., 2018) achieves a convincing correlation between WLs and RIs of
365 moderate-to-strong earthquakes on the Dead Sea fault. Whereas the fault system along the Dead
366 Sea fault is more complicated, three-dimensional modeling of the tectonic motion, coupled with
367 the pore pressure evolution, may give more reliable predictions regarding earthquake ruptures and
368 their chronology. However, based on the relationship between the WL and RI changes presented
369 in this article, with the current anthropogenic decrease in the Dead Sea level (with an average
370 annual rate of ~ 1 m / yr), a moderate to severe earthquake will not be triggered by the mechanism
371 discussed here. This article not only suggests the existence of a connection between WL and RI,
372 but also provides additional guidance based on this connection.

373 **DATA AVAILABILITY**

374 All raw data can be provided by the corresponding authors upon request.

375 **AUTHOR CONTRIBUTIONS**

376 MB and AA Conceptualization; AA data collection and analysis; MB Modelling, data
377 visualization and results analysis; RK Validation; MB original draft preparation; MB, RK and AA
378 review and revisions; AA, ZB and RK Funding acquisition and Resources.

379 **COMPETING INTERESTS**

380 The authors declare that they have no conflict of interest.

381 **ACKNOWLEDGMENTS**

382 This project was supported by grants from the Ministry of Natural Infrastructures, Energy
383 and Water Resources of Israel # 213-17-002, GIF- German - Israeli Foundation for Scientific
384 Research and Development # I-1280-301.8, and by PhD fellowships from the University of Haifa,
385 Israel. The data for this paper were obtained with analytical and numerical modeling.

386 **REFERENCE**

387 Agnon, A.: Pre-instrumental earthquakes along the Dead Sea rift. In Dead Sea transform fault
388 system: Reviews, edited by: Garfunkel, Z., Ben-Avraham, Z., Kagan, E., Springer,
389 Dordrecht, Netherlands, 207-261, https://doi.org/10.1007/978-94-017-8872-4_8, 2014.

390 Ambraseys, N.: Earthquakes in the Mediterranean and Middle East: a multidisciplinary study of
391 seismicity up to 1900. Cambridge University Press. doi:
392 <https://doi.org/10.1017/CBO9781139195430>, 2009.

393 Ambraseys, N., Melville, C. P. and Adams, R. D.: The Seismicity of Egypt, Arabia and the Red
394 Sea: A Historical Review. Cambridge: Cambridge Univ. Press.
395 <https://doi.org/10.1017/S1356186300007240>, 1994.

396 Amiran, D. H., Arieh, E., and Turcotte, T.: Earthquakes in Israel and adjacent areas: macroscopic
397 observations since 100 B.C.E. *Isr. Explor. J.*, 44, 260– 305.
398 <http://www.jstor.org/stable/27926357>, 1994.

399 Anderson, E. M.: The dynamics of faulting (2nd Edition), edited by: Oliver and
400 Boyd, Edinburgh, Scotland, 206, <https://doi.org/10.1144/transed.8.3.387>, 1951.

401 Avni, R., Bowman, D., Shapira, A. and Nur, A.: Erroneous interpretation of historical documents
402 related to the epicenter of the 1927 Jericho earthquake in the Holy Land, *J. Seismol.*, 6(4),
403 469-476. <https://doi.org/10.1023/A:1021191824396>, 2002.

404 Baer G., Funning, G. J., Shamir, G. and Wright T. J.: The 1995 November 22, Mw 7.2 Gulf of Elat
405 earthquake cycle revisited, *Geophys. J. Int.*, 175(3), 1040-
406 1054, <https://doi.org/10.1111/j.1365-246X.2008.03901.x>, 2008.

407 Belferman, M., Katsman, R. and Agnon, A. Effect of large-scale surface water level fluctuations
408 on earthquake recurrence interval under strike-slip faulting. *Tectonophysics*, 744, 390-402.
409 <https://doi.org/10.1016/j.tecto.2018.06.004>, 2018.

410 Ben-Menahem, A.: Earthquake catalogue for the Middle East (92 BC-1980 AD), *B. Geofis. Teor.*
411 *Appl.*, 21, 245-313, 1979.

412 Bookman, R., Enzel, Y., Agnon, A., and Stein, M.: Late Holocene lake levels of the Dead Sea,
413 *GSA Bulletin*, 116, 555-571, <https://doi.org/10.1130/B25286.1>, 2004.

414 Byerlee, J.D.: Friction of rocks. In: Byerlee, J.D., Wyss, M. (Eds.), *Rock Friction and Earthquake*
415 *Prediction*. Springer, Birkhäuser, Basel, 615–626, [https://doi.org/10.1007/978-3-0348-](https://doi.org/10.1007/978-3-0348-7182-2)
416 [7182-2](https://doi.org/10.1007/978-3-0348-7182-2), 1978.

417 Durá-Gómez, I. and Talwani, P.: Reservoir-induced seismicity associated with the Itoiz Reservoir,
418 Spain: a case study, *Geophys. J. Int.*, 181, 343–356, [https://doi.org/10.1111/j.1365-](https://doi.org/10.1111/j.1365-246X.2009.04462.x)
419 [246X.2009.04462.x](https://doi.org/10.1111/j.1365-246X.2009.04462.x), 2010.

420 Elad, A.: An early Arabic source concerning the markets of Jerusalem. *Cathedra*, 24, 31-40, 1982.

421 Elad, A.: Two Identical Inscriptions From Jund Filastin From the Reign of the Abbāsid Caliph,
422 Al-Muqtadir, J. Econ. Soc. Hist. Orie., 35(4), 301-360, <https://doi.org/10.2307/3632739>,
423 1992.

424 Garfunkel, Z.: Lateral motion and deformation along the Dead Sea Transform, in: Dead Sea
425 Transform Fault System: Reviews, edited by: Garfunkel, Z., Ben-Avraham, Z., Kagan, E.,
426 Springer, Dordrecht, Netherlands, pp. 109–150. [http://dx.doi.org/10.1007/978-94-017-](http://dx.doi.org/10.1007/978-94-017-8872-4)
427 [8872-4](http://dx.doi.org/10.1007/978-94-017-8872-4), 2014.

428 Gerber, H.: " Palestine" and Other Territorial Concepts in the 17th Century, Int. J. Middle E.
429 Stud., 30(4), 563-572. <https://www.jstor.org/stable/164341>, 1998.

430 Guidoboni, E., Comastri, A. and Traina, G.: Catalogue of Ancient Earthquakes in the
431 Mediterranean Area Up to the 10th Century, Istituto nazionale di geofisica, Rome, Italy,
432 <https://doi.org/10.1163/182539185X01377>, 1994.

433 Guidoboni, E. and Comastri, A.: Catalogue of Earthquakes and Tsunamis in the Mediterranean
434 Area from the 11th to the 15th Century. Istituto nazionale di geofisica e Vulcanologia,
435 Rome, Italy, <https://doi.org/10.1515/BYZS.2008.854>, 2005.

436 Gupta, H. K: A review of recent studies of triggered earthquakes by artificial water reservoirs with
437 special emphasis on earthquakes in Koyna, India, Earth-Sci. Rev., 58(3-4), 279-310,
438 [https://doi.org/10.1016/S0012-8252\(02\)00063-6](https://doi.org/10.1016/S0012-8252(02)00063-6), 2002.

439 Gupta, H., K.: Reservoir triggered seismicity (RTS) at Koyna, India, over the past 50 yrs, B.
440 Seismol. Soc. Am., 108, 2907-2918, <https://doi.org/10.1785/0120180019>, 2018.

441 Hamiel, Y., Masson, F., Piatibratova, O. and Mizrahi, Y.: GPS measurements of crustal
442 deformation across the southern Arava Valley section of the Dead Sea Fault and

443 implications to regional seismic hazard assessment. *Tectonophysics*, 724, 171-178.
444 <https://doi.org/10.1016/j.tecto.2018.01.016>, 2018.

445 Hamiel, Y. and Piatibratova, O.: Style and distribution of slip at the margin of a pull-apart
446 structure: Geodetic investigation of the Southern Dead Sea Basin. *J. Geophys. Res.-Sol.*
447 *Ea.*, 124(11), 12023-12033. <https://doi.org/10.1029/2019JB018456>, 2019.

448 Hofstetter, R., Klinger, Y., Amrat, A. Q., Rivera, L. and Dorbath, L.: Stress tensor and focal
449 mechanisms along the Dead Sea fault and related structural elements based on
450 seismological data. *Tectonophysics*, 429(3-4), 165-181.
451 <https://doi.org/10.1016/j.tecto.2006.03.010>, 2007.

452 Hua, W., Chen, Z. and Zheng, S.: Source parameters and scaling relations for reservoir induced
453 seismicity in the Longtan reservoir area. *Pure Appl. Geophys.* 170, 767–783.
454 <https://doi.org/10.1007/s00024-012-0459-7>, 2013a.

455 Hua, W., Chen, Z., Zheng, S., and Yan, C.: Reservoir-induced seismicity in the Longtan
456 reservoir, southwestern China. *J. Seismol.* 17 (2), 667–681.
457 <https://doi.org/10.1007/s10950-012-9345-0>, 2013b.

458 Hough, S. E. and Avni, R.: The 1170 and 1202 CE Dead Sea Rift earthquakes and long-term
459 magnitude distribution of the Dead Sea Fault Zone, *Israel J. Earth Sci.*, 58, 295–308.
460 <https://doi.org/10.1560/IJES.58.3-4.295>, 2011.

461 Jaeger, J., Cook, N. G. and Zimmerman, R.: *Fundamentals of rock mechanics*, fourth edition,
462 Blackwell Publishing, Oxford, UK, 2009.

463 Kagan, E., Stein, M., Agnon, A., and Neumann, F.: Intrabasin paleoearthquake and quiescence
464 correlation of the late Holocene Dead Sea, *J. Geophys. Res.-Sol. Ea.*, 116(B4), 148-227,
465 <https://doi.org/10.1029/2010JB007452>, 2011.

466 Ken-Tor, R., Agnon, A., Enzel, Y., Stein, M., Marco, S. and Negendank, J. F.: High-resolution
467 geological record of historic earthquakes in the Dead Sea basin, *J. Geophys. Res.-Sol. Ea.*,
468 106, 2221-2234, <https://doi.org/10.1029/2000JB900313>, 2001.

469 Langgut, D., Yannai, E., Taxel, I., Agnon, A. and Marco, S.: Resolving a historical earthquake
470 date at Tel Yavneh (central Israel) using pollen seasonality. *Palynology*, 40(2), 145-159,
471 <https://doi.org/10.1080/01916122.2015.1035405>, 2015.

472 Lefevre, M., Klinger, Y., Al-Qaryouti, M., Le Béon, M. and Moumani, K.: Slip deficit and
473 temporal clustering along the Dead Sea fault from paleoseismological investigations. *Sci.*
474 *Rep.-UK*, 8 (1), 4511. <https://doi.org/10.1038/s41598-018-22627-9>, 2018.

475 Lyakhovsky, V., Ben-Zion, Y., Agnon, A.: Earthquake cycle, fault zones, and seismicity patterns
476 in a rheologically layered lithosphere, *J. Geophys. Res.-Sol. Ea.*, 106 (B3), 4103–4120,
477 <https://doi.org/10.1029/2000JB900218>, 2001.

478 Marco, S., Stein, M., Agnon, A., and Ron, H.: Long-term earthquake clustering: A 50,000-year
479 paleoseismic record in the Dead Sea Graben, *J. Geophys. Res.-Sol. Ea.*, 101(B3), 6179-
480 6191. <https://doi.org/10.1029/95JB01587>, 1996.

481 Masson, F., Hamiel, Y., Agnon, A., Klinger, Y. and Deprez, A.: Variable behavior of the Dead
482 Sea Fault along the southern Arava segment from GPS measurements, *C.R.*
483 *Geosci.*, 347(4), 161-169. <https://doi.org/10.1016/j.crte.2014.11.001>, 2015.

484 Migowski, C., Agnon, A., Bookman, R., Negendank, J. F., and Stein, M.: Recurrence pattern of
485 Holocene earthquakes along the Dead Sea transform revealed by varve-counting and
486 radiocarbon dating of lacustrine sediments: *Earth Planet. Sc. Lett.*, 222, 301– 314.
487 <https://doi.org/10.1016/j.epsl.2004.02.015>, 2004.

488 Migowski, C., Stein, M., Prasad, S., Negendank, J. F. W., and Agnon, A.: Holocene climate
489 variability and cultural evolution in the Near East from the Dead Sea sedimentary record.
490 *Quaternary Res.*, 66(3), 421-431, <https://doi.org/10.1016/j.yqres.2006.06.010>, 2006.

491 Mogi, K.: Some discussions on aftershocks, foreshocks and earthquake swarms: the fracture of a
492 semi-infinite body caused by an inner stress origin and its relation to the earthquake
493 phenomena (third paper), *B. Earthq. Res. I. Tokyo*, 41(3), 615-658, 1963.

494 Palano, M., Imprescia, P., and Gresta, S.: Current stress and strain-rate fields across the Dead Sea
495 Fault System: Constraints from seismological data and GPS observations, *Earth Planet. Sc.*
496 *Lett.*, 369, 305-316. <https://doi.org/10.1016/j.epsl.2013.03.043>, 2013.

497 Pandey, A.P. and Chadha, R.K.: Surface loading and triggered earthquakes in the Koyna–Warna
498 region, western India, *Phys. Earth Planet. In.* 139 (3–4), 207–223.
499 <http://dx.doi.org/10.1016/j.pepi.2003.08.003>, 2003.

500 Parker, S.T.: Preliminary Report on the 1980 Season of the Central" Limes Arabicus" Project, *B.*
501 *Am. Sch. Oriental Re.*, 247(1), pp.1-26.
502 <https://www.journals.uchicago.edu/doi/10.2307/1356476>, 1982.

503 Rao, N. P., and Shashidhar, D.: Periodic variation of stress field in the Koyna–Warna reservoir
504 triggered seismic zone inferred from focal mechanism studies. *Tectonophysics*, 679, 29-
505 40, <https://doi.org/10.1016/j.tecto.2016.04.036>, 2016.

506 Roeloffs, E. A.: Fault stability changes induced beneath a reservoir with cyclic variations in water
507 level, *J. Geophys. Res.-Sol. Ea.*, 93, 2107-2124,
508 <https://doi.org/10.1029/JB093iB03p02107>, 1988.

509 Russell, K. W.: The earthquake chronology of Palestine and northwest Arabia from the 2nd
510 through the mid-8th century AD, *B. Am. Sch. Oriental Re.*, 260(1), 37-59,
511 <https://doi.org/10.2307/1356863>, 1985.

512 Sadeh, M., Hamiel, Y., Ziv, A., Bock, Y., Fang, P. and Wdowinski, S.: Crustal deformation along
513 the Dead Sea Transform and the Carmel Fault inferred from 12 years of GPS
514 measurements, *J. Geophys. Res.-Sol. Ea.*, 117(B8), 410,
515 <http://dx.doi.org/10.1029/2012JB009241>, 2012.

516 Scholz, C. H.: Crustal movements in tectonic areas. *Tectonophysics*, 14(3-4), 201-217.
517 [https://doi.org/10.1016/0040-1951\(72\)90069-8](https://doi.org/10.1016/0040-1951(72)90069-8), 1972.

518 Shapira, A., Avni, R., and Nur, A.: A new estimate for the epicenter of the Jericho earthquake of
519 11 July 1927. *Israel J. Earth Sci.*, 42(2), 93-96, 1993.

520 Simpson, D. W.: Seismicity changes associated with reservoir loading. *Eng. Geol.*, 10(2-4), 123-
521 150. [https://doi.org/10.1016/0013-7952\(76\)90016-8](https://doi.org/10.1016/0013-7952(76)90016-8), 1976.

522 Simpson, D. W., Leith, W., and Scholz, C.: Two types of reservoir-induced seismicity, *B. Seismol.*
523 *Soc. Am.*, 78, 2025–2040, 1988.

524 Snow, D. T.: Hydrogeology of induced seismicity and tectonism: Case histories of Kariba and
525 Koyna, *Geol. S. Am. S.*, 189, 317-360,
526 <https://doi.org/10.1130/SPE189-p317>, 1982.

- 527 Stern, O.: Geochemistry, Hydrology and Paleo-Hydrology of Ein Qedem Spring System; Report
528 GSI/17/2010, Geological Survey of Israel, Jerusalem, Israel, p. 91 (In Hebrew), 2010.
- 529 Talwani, P.: On the nature of reservoir-induced seismicity. *Pure Appl. Geophys.*, 150, 473–492,
530 https://doi.org/10.1007/978-3-0348-8814-1_8, 1997.
- 531 Wang, H.: *Theory of Linear Poroelasticity with Applications to Geomechanics and Hydrogeology*,
532 University Press, Princeton, 2000.
- 533 Wechsler, N., Rockwell, T. K., Klinger, Y., Štěpančíková, P., Kanari, M., Marco, S., and Agnon,
534 A.: A paleoseismic record of earthquakes for the Dead Sea transform fault between the first
535 and seventh centuries CE: Nonperiodic behavior of a plate boundary fault, *B. Seismol. Soc.*
536 *Am.*, 104(3), 1329-1347. <https://doi.org/10.1785/0120130304>, 2014.
- 537 Williams, J. B., Schwab, M. J., & Brauer, A.: An early first-century earthquake in the Dead
538 Sea, *Int. Geol. Rev.*, 54(10), 1219-1228, <https://doi.org/10.1080/00206814.2011.639996>,
539 2012.

540 **Appendix: The earthquake history of the Dead Sea environs**

541 Numerous publications list earthquakes that hit the Dead Sea and its surroundings during the last
542 two millennia (e.g. Agnon, 2014; Ambraseys et al., 1994; Ambraseys, 2009; Amiran et al., 1994;
543 Guidoboni et al., 1994, Guidoboni and Comastri, 2005). In Belferman et al. (2018) we adopted
544 from the scores of listed events only the most destructive ones, typically causing local intensities
545 of VII or higher in Jerusalem. For a minimal epicentral distance of 30 km, this would translate to
546 a magnitude of ~5.7 or higher (according to the attenuation relation of Hough and Avni, 2011).

547 Table A1 lists the Dead Sea earthquakes considered for stress release across the Dead Sea basin
548 during the last two millennia. We used two criteria: noticeable damage in fortified Jerusalem, and
549 seismites in the northern Dead Sea. Our simple model simulates an earthquake time series, given
550 a water level curve. Eleven events from this time series correlate with events of magnitude ~6 or
551 more in the historical record. Yet, the model generates four events that are not included in our
552 original catalog. On the other hand, a single event (~660 CE) listed in Belferman et al. (2018) has
553 no counterpart in the simulations despite a wide range of level curves tested. All these curves are
554 generated by a random number generator, subject to constraints from field data. We first discuss
555 the four events required by the simulations one by one. Then we review the ~660 CE event along
556 with other historical events that were left out already in Belferman et al. (2018).

557 The earthquakes in Table 1 are classified according to the level of acceptance for being destructive
558 in Jerusalem. The nine events of **Class C** are all consensual, also used by Belferman et al. (2018).
559 These events appear in all catalogs and lists and need no further discussion. The six events of **Class**
560 **A** are debated events, accepted in the present study. All earthquakes in this class are selected by
561 simultaneously satisfying two criteria: (1) The acceptance regularizes the relation between
562 recurrence intervals and lake level; (2) They are corroborated by evidence from seismites in the
563 northern basin of the Dead Sea (Ein Feshkha and Ein Gedi sites, Fig.A1 corroborate).

564 We chose the year **33** CE to start our simulations. While this earthquake did not cause a widespread
565 damage, it was recorded in all three seismite sites (Kagan et al., 2011), with a maximum of decade
566 uncertainty based on dating by counting lamina under the microscope (Migowski et al., 2004;
567 Williams et al., 2012).

568 The second entry in Table A1, **~100** CE, refers to two decades of unrest. Migowski et al. (2004)
569 identified a pair of seismites around 90 CE and 112 CE in the 'Ein Gedi Core. The corresponding

570 sequences in Ein Feshkha and Ze'elim Creek are laminates, attesting to quiescence. A historical
571 hiatus between the Roman demolition of Jerusalem and the erection of Ilya Capitolina in its stead
572 (70-130 CE) preclude historical evidence. Although damage to the Masada fortress has been
573 assigned to an earthquake **1712 CE**.

574 Table A2 lists ten earthquakes that have been reported to damage around Jerusalem but are not
575 required by our simulations. The seven events of **Class R** are the debated events, rejected here
576 after discussion. The three **Class S** events were skipped altogether in that compilation of
577 Ambraseys (2009).

578 Of the seven Class R events, the 7 June **659 CE** earthquake was accepted by us in Belferman et al.
579 (2018). The earthquake has been associated with destruction of the Euthymius monastery 10 km
580 east of Jerusalem, but no damage in the town of Jerusalem has been unequivocally reported
581 (Ambraseys, 2009). In Belferman et al. (2018) we included this event in the catalog of Dead Sea
582 earthquakes, as Langgut et al. (2015) have located it on the center of the Jordan Valley segment of
583 the transform (Figure A1). However, this interpretation neglected the possibility that the rupture
584 could have been outside the hydrological effect of the Dead Sea basin. One of the lessons of our
585 numerous simulations is that our model would not support triggering of this earthquake shortly
586 (less than a century) before the mid-8th century crisis, when lake levels were dropping to the lowest
587 point in the studied period (420 m bsl, Figure 1a). When rejecting the 659 CE event, the 419 CE
588 earthquake is the one preceding the mid-8th century crisis; the three century recurrence interval
589 fits well the low lake level.

590 **1016 CE**: The collapse of the Dome of the Rock was not explicitly attributed to an earthquake by
591 the original sources, who found it enigmatic as well (Ambraseys, 2009).

592 **1644 CE:** Ambraseys (2009) quoted a late Arab author, al-Umari, who reported collapse of houses
593 and deaths of five persons in “the town of Filistin”. While Ambraseys has interpreted it probably
594 to Jerusalem, it might refer to al-Ramla, the historical capital of the classical Filistin District, as in
595 “al-Ramla, Madinat Filastin” (Elad, 1992, p335). Or, it is a mistranslation of “Bilad Filistin” which
596 at that time started refer to the entire Holy Land district, without specifying a town (Gerber, 1998).
597 Jerusalem, at that time, was called Bayt el Maqdis or, as nowadays, al-Quds. The only report of an
598 earthquake in Jerusalem around 1644 mentions horror but no structural damage - the 1643 CE
599 event that Ambraseys (2009) tends to equate with the 1644 CE event. A seismite in Ein Gedi core
600 can be correlated with this event (Migowski et al., 2004, Table 2, entry 6). Migowski et al. (2004)
601 have identified the seismite with the 1656 earthquake that was felt in Palestine; Ambraseys’ (2009)
602 interpretation was not yet available for them.

603 **1656 CE:** This event was strong in Tripoli and only felt in Palestine. Migowski et al. (2004)
604 correlated it to a seismite based on deposition rates (no lamina counting for that interval). Given
605 the 1644 CE entry of Ambraseys (2009), this interpretation should be revised, and the 1656 CE
606 earthquake is not to be associated with any local rupture in the Dead Sea.

607
608
609
610

Table A1: A catalog of earthquakes that could potentially damage Jerusalem. The classes denote the level of acceptance of damage to Jerusalem among the researchers: C - consensual; B - accepted by Belferman et al., 2018; A - amended here; R - rejected here.

Year CE or Century (marked C)	Class	Seismite correl. by site			Reference	Comments
		Z E †	E G ^Y	E F ^o		
33	B	+	+	+	MI,K&,W&	Identified in all three seismites sites, varve-counted to 31 BCE
100~	B	-	2	-	MI,AM	Seismites ~90 and ~112; questionable archaeological evidence
~175	B	-	+	-	MI	A seismite; no historical or archeological support
363	C	-	-	+	K&,A&	A seiche in the Dead Sea, a seismite at EF° (north Dead Sea)
419	C	+	+	+	KT/MI/K&	
551	A	+	+	+	PA,AM	
747/9,757	C	+	+	+	KT/MI/K&	
1033	C	?	+	+	KT/MI/K&	
~1150	A	+	-	/	AM,K&	I ₀ IX - Mar Elias (& Qasr al-Yahud) monasteries demolished
1293	C	+	+	+	K&	
1458	C	+	+	h	MI	
1546	C	/	+	i	MI	
1712	A	/	+	a	MI	A& / I ₀ VII - “ruined three Turkish houses in Jerusalem”
1834	C	+	+	t	KT,MI	
1903	R	m	m	u	A&,AM	I ₀ VII Mt. of Olives; several shocks, I ₀ up to VII over a large area
1927	C	+	+	s	KT,MI	AV / I ₀ VII-VIII in and around Jerusalem (I ₀ 7.8 by GMPE)

611
612
613
614
615

616
617
618

Table A2: Events listed in some catalogs and subsequently skipped (Class S) or declined (Class D) by Ambraseys (2009), or rejected (Class R) in the present study.

Year CE	C l a s s	Seismite correl. by site			Reference	Comments
		Z E †	E G ^Y	E F °		
~659	R	-	+	+	L&,AM	Jordan Valley, possibly over 65 km NE of Jerusalem
808	S	/	-	?	A&	
1016	D	?	?	?	AM,A&	Damage to the Dome of Rock, no specific reference to shaking
1042	S	-	+	-	BM	Syria, off the Dead Sea transform
1060	S	/	-	+	A&,SB	The roof of Al-Aqsa collapsed
1063	R				A&,AM,SB	Syrian littoral
1068	D	+	+	+	AM	Neither of the two events can be associated with the Dead Sea
1105	D	?	?	?	A&,AM	“Strong” but “no damage recorded in the sources”
1114	D	+	+	?	A&,AM	1114 - no damage around the city, a swarm, Kingdom’s north
~1117	R	+		?	A&,AM	
1557	R				Am	Collapse in Jerusalem: a gun foundry, a forgery, an oven
1644	R	h	+*	h	Am	Some damage and death toll in Palestine, likely Seismite 6 of MI
1656	R	h	-	h	A&,AM,SB	Tripoli VII, Palestine IV, MI misidentified with Seismite 6
1817	R				AM	Two churches damaged in Jerusalem, Holy Sepulchre affected
1870	S	?	-	h	AM	Mediterranean source

619 Abbreviations and notes:

620 †ZE - Ze' elim Creek; ‡EG - Ein Gedi core; °EF - Ein-Feshkha Nature Reserve

621 AM: Ambraseys, 2009; A&: Amiran et al., 1994; K&: Kagan et al., 2011; L&: Langgut et al.

622 2015; KT: Ken-Tor et al., 2004; MI: Migowski et al., 2004; PA: Parker, 1982; W&: Williams et

623 al., 2012.

624

625

626

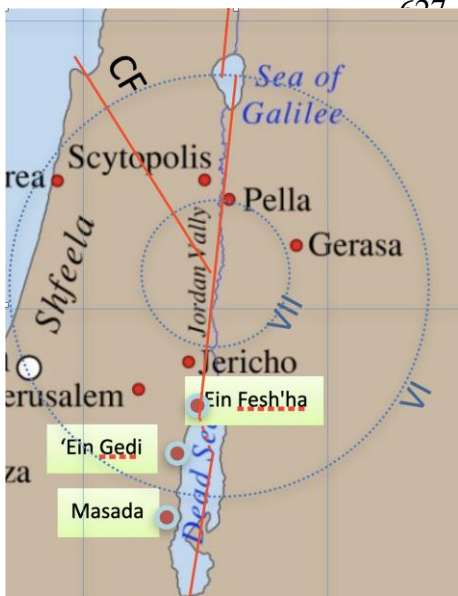


Figure A1: A map showing the epicenter reconstructed by Langgut et al. (2015) for the 659/660 CE mainshock.